JOURNAL OF GEOPHYSICAL RESEARCH, VOL. 113, D14306, doi:10.1029/2007JD009498, 2008

Model bias correction for dust storm forecast using ensemble Kalman filter

Caiyan Lin,[1,2] Jiang Zhu,[1] and Zifa Wang[1]

Received 13 October 2007; revised 19 December 2007; accepted 11 March 2008; published 22 July 2008.

[1] First attempt to correct model bias in a dust transport model using ensemble Kalman filter (EnKF) assimilation targeting heavy dust episodes during the period of 15–24 March 2002 over north China is successfully performed. The uncertainty of dust emissions and surface wind fields are taken into account individually and simultaneously to correct their biases. The 24-h surface forecasts are significantly improved with the root mean square error reduced by more than 45% on 20 March and by 50% on 21 March after correcting the biases. The results indicate that there are high biases due to the dust emissions and surface wind fields. These biases converge to the values similar with those obtained in previous sensitivity analyses indicating that the EnKF can accurately correct the bias. The corrected total dust emissions are decreased more than 33%. However, when considered simultaneously, they do not converge to the same results as those considered individually. This indicates that the two biases can compensate for each other in terms of predicted surface dust concentration.

Citation: Lin, C., J. Zhu, and Z. Wang (2008), Model bias correction for dust storm forecast using ensemble Kalman filter, *J. Geophys. Res.*, *113*, D14306, doi:10.1029/2007JD009498.

1. Introduction

[2] Dust storms have drawn much concern during the past two decades due to their strong impacts on atmospheric environment, biogeochemical cycles, radiative balance and human health. Observations and numerical model simulations are important for improving our understanding of recently increasing Asian dust episodes. Dust observations are still sparse, while numerical models can provide space-time forecasts regularly with high resolution and have reproduced many important observational facts. However, numerical forecasts of dust storms will suffer from uncertainties in initial conditions and the model itself. Previous study on dust-storm data assimilation [*Lin et al.*, 2008a], which can maximize reduction of the uncertainty in the initial conditions (initial uncertainty), shows the merit of ensemble Kalman filter (EnKF) in mesoscale system. Also, it also suggests that forecast errors are mainly contributed by uncertainty in the model itself (model uncertainty), including their biases (systematic error), rather than the error in initial condition.

[3] Recently, several regional models applied to the ACE-Asia field observation period [*Gong et al.*, 2003; *Huebert et al.*, 2003] found that the estimated dust emission fluxes differ greatly, and the predicted surface level dust concentrations from models, which have very similar transport patterns from the emission source region, sometimes are different by more than two orders of magnitude. Such wide variety reflects large model uncertainty in the dust emission scheme, the input data (land-use data, meteorological fields, etc.) and the numerical approximation. Moreover, the results of the recent dust model intercomparison project (DMIP) [*Uno et al.*, 2006] indicate that modeled dust emissions over the Gobi Desert region differ by a factor of 10 among the models; wind speeds are highly uncertain in the source area; and the modeled dust transport and removal processes are significant after the dust clouds depart the continent.

[4] Therefore it is important to account for the model uncertainty and correct their biases to improve the dust forecast. Simply comparing model forecasts to observations cannot separate the initial uncertainty and the model uncertainty. In other words, these comparisons do not give information on the associated uncertainty. The best way to characterize the uncertainty would be the probability density functions (PDF) of the simulation errors. However, it is difficult to compute the full PDF for given forecast error statistics primarily because of the computational costs. There are several methods to estimate the uncertainty. The first-order derivatives of model outputs with respect to model inputs can provide ''local'' estimates of uncertainty [*Schmidt*, 2002]. Monte Carlo simulations with different values for given input parameters or fields can approximate the PDF if the ensemble number is large enough [*Hanna et al.*, 2001]. An ensemble approach based on a set of models is an alternative approach to account for the range of uncertainty [*Mallet and Sportisse*, 2006].

[5] Ensemble Kalman filter (EnKF) [*Evensen*, 2006, and reference therein] uses the Monte Carlo ensembles (can be extended to multimodels) to approximate the error statistics used to integrate observations into the model. The EnKF

[1]LAPC and NZC, Institute of Atmospheric Physics, Chinese Academy of Sciences, Beijing, China.
[2]Graduate University of Chinese Academy of Sciences, Beijing, China.

0148-0227/08/2007JD009498$09.00

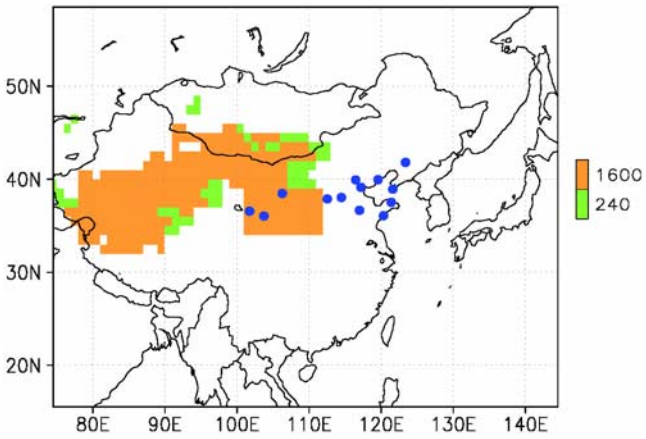

Figure 1. Modeling domain, the weighting factor (C_1) (shaded) for desert and bare ground, and observation stations of PM_{10} from SEPA on 22 March (blue dots).

cannot only account for the range of uncertainty as in the ensemble approach but can also correct the model bias by assimilating the observations. In addition, it can avoid filter divergence reasonably by considering the model uncertainty from the view of assimilation. This paper uses EnKF to correct the model biases and to demonstrate their impacts on dust-storm forecast and assimilation targeting the heavy dust episodes during 15–24 March 2002.

[6] The next section describes the model and observational data including the quality control, while the method of EnKF and the details of experimental configuration are presented in section 3. Section 4 discusses the results. Conclusions are drawn in last section.

2. Descriptions of Model and Observation Data

2.1. Model Description and Setting

[7] The regional dust transport model included deflation, transport, diffusion, and removal processes during the life cycle of the yellow sand particles. This model has been successfully used to study atmospheric trace gases and particles, such as SO_x, dust, O_3 and acid rain over East Asia [*Wang et al.*, 2000, 2002; *Uematsu et al.*, 2003]. In this study, nine bin dust particles (0.5–90 μm in radius) are modeled. The dust emission intensity $Q_{i,j,l}$ in the l-th size bin at location i, j depends on the conditions at the lowest model level and is given by

$$Q_{i,j,l} = C_1 C_2 u^{*2}_{i,j,l} \left(1 - u^{*}_{0i,j,l}/u^{*}_{i,j,l}\right) W_{i,j,l} R_{i,j,l} \qquad (1)$$

Where $Q_{i,j,l}$ is given as kg m^{-2} s^{-1}, C_1 is the weighting factor for different land types (C_1 for desert and bare ground are shown in Figure 1), and C_2 is the empirical constant set as 2.9×10^{-2}. $u^{*}_{i,j,l}$ is the friction velocity, and $u^{*}_{0i,j,l}$ is the threshold value of friction velocity (0.4 m/s). $R_{i,j,l}$ is the fraction of the l-th bin of deflating yellow sand, $W_{i,j,l}$ is the humidity factor, which is assumed to be linearly dependent on the relative humidity (RH) as

$$W_{i,j,l} = \begin{cases} (1 - \mathrm{RH}/\mathrm{RH}_0) & \text{for} \quad \mathrm{RH} < \mathrm{RH}_0 \\ 0 & \text{for} \quad \mathrm{RH} \le \mathrm{RH}_0 \end{cases} \qquad (2)$$

where RH and RH_0 are the surface relative humidity and its critical value (40%). The simulation domain used ranges from (75°E, 16°N) to (146°E, 60°N) consisting of 72 by 45 grid cells horizontally (Figure 1) and 18 vertical layers in terrain-following coordinates. Details about the model are discussed by *Wang et al.* [2000].

Table 1. Number of Quantified PM_{10} Data After Quality Control Over North China During 15–24 March 2002

March 2002	15	16	17	18	19	20	21	22	23	24
Observations	0	4	7	4	0	6	12	13	5	0

Table 2. Comparison Experiments

Experiments	Assimilation	Inflation	Assimilation With Parameter α_Q	Assimilation With Parameter α_V
Reference	×			
Inflation	✓	✓		
Emis	✓		✓	
Wind	✓			✓
Emis + wind	✓		✓	✓

2.2. Observation Data

[8] Daily averaged PM_{10} observations in China are used for assimilation and validation. In order to remove the likely impact of anthropogenic pollution and examine the impact of model biases on heavy dust episodes, before use, the observations are checked according to 3 h surface synoptic observations of dust phenomenon from. If there are at least three occurrences of floating dust, or a combination of one floating dust and one blowing dust, or one dust storm phenomenon observed at stations located within one latitude degree around the PM_{10} station during the day, the PM_{10} observations of this station are considered as mainly contributed by dust, and thus selected. Otherwise the data

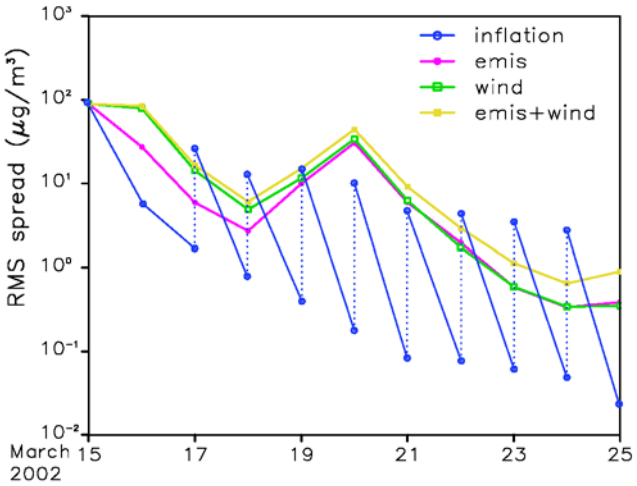

Figure 2. RMS spread (RMSS) of the ensembles. Blue line gives the RMSS before and after inflation linked by the dotted line. The pink, green, and yellow lines show the results for the schemes "emis", "wind", and "emis + wind", respectively.

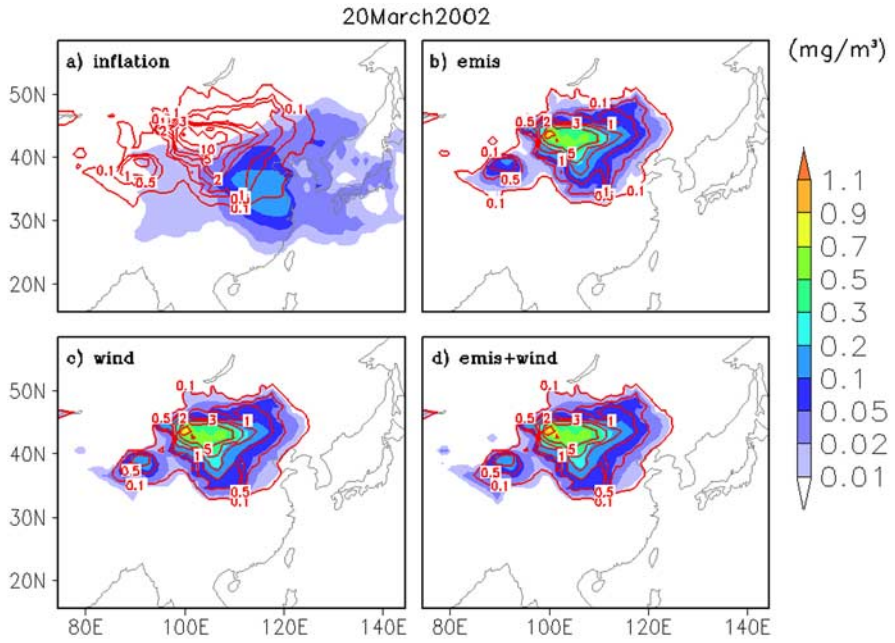

Figure 3. Shaded areas indicate the horizontal distribution of surface estimated forecast error (spread) for scheme (a) "inflation", (b) "emis", (c) "wind", and (d) "emis + wind" on 20 March. The contours indicate the ensemble mean of the background dust concentrations for each scheme.

would be discarded. The number of qualified PM_{10} observations after quality control are listed in Table 1, clearly indicating the influence of dust storms. The distribution of most qualified PM_{10} observations on 22 March is shown in Figure 1. Although the observations of PM_{10} used here are limited, using fewer but higher quality observations is better than using more but lower quality observations. Since other potential observations such as visibility measurements need

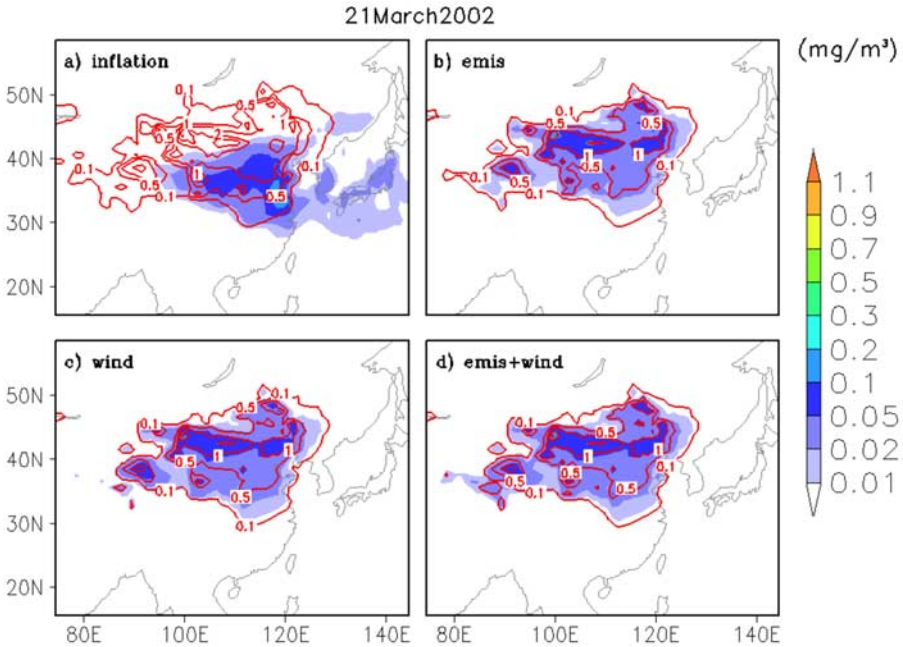

Figure 4. As in Figure 3 but on 21 March 2002.

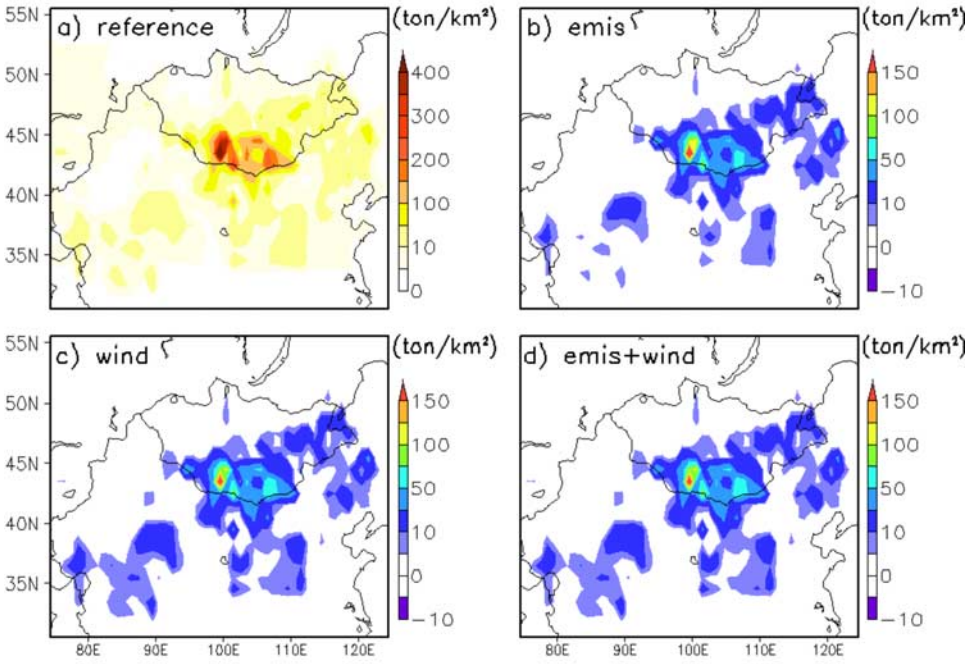

Figure 5. Horizontal distribution of estimated dust emission intensity for without data assimilation (a) and the difference betweens situations without and with bias correction (b, c, and d).

heavy quality control, this paper does not include assimilation of visibility observations.

[9] The boundary layer averaged dust extinction coefficients at Beijing, China from the NIES lidar observations [*Sugimoto et al.*, 2003] are also used for comparison.

3. EnKF and Experimental Details

3.1. Method of EnKF

[10] The basic idea of the EnKF [*Evensen*, 1994] is to construct a Monte Carlo ensemble such that the mean of the ensemble is the best estimate, and the ensemble error covariance is a good estimate of the forecast error covariance.

[11] At the current assimilation time t (for notational simplicity, the t time subscript will be dropped), we assume that we have an ensemble of forecasts that randomly sample the forecast errors, denoted by $\mathbf{X}^{\mathrm{b}} = (\mathbf{x}_1^{\mathrm{b}}, \mathbf{x}_2^{\mathrm{b}}, \cdots, \mathbf{x}_N^{\mathrm{b}})$ whose columns are composed of ensemble member of model state vectors. Then the estimated forecast error covariance $\hat{\mathbf{P}}^{\mathrm{b}}$ used in the EnKF is randomly sampled from this finite ensemble:

$$\hat{\mathbf{P}}^{\mathrm{b}} = \frac{1}{N-1}\mathbf{X}'^{\mathrm{b}}\mathbf{X}'^{\mathrm{bT}} = \frac{1}{N-1}\left(\mathbf{X}^{\mathrm{b}} - \bar{\mathbf{X}}^{\mathrm{b}}\right)\left(\mathbf{X}^{\mathrm{b}} - \bar{\mathbf{X}}^{\mathrm{b}}\right)^{\mathrm{T}} \quad (3)$$

The ensemble mean $\bar{\mathbf{X}}^{\mathrm{b}}$ is defined by $\bar{X}^{\mathrm{b}} = \bar{\mathbf{X}}^{\mathrm{b}} = \frac{1}{N}\sum_{i=1}^{N} \mathrm{x}_i^{\mathrm{b}}$, and the ensemble perturbation from the mean for i-th member is $\mathbf{x}_i'^{\mathrm{b}} = \mathbf{x}_i^{\mathrm{b}} - \bar{\mathbf{x}}^{\mathrm{b}}$.

[12] The EnKF performs an ensemble of parallel data assimilation cycles, i = 1, ... , N, so that each member is updated to somewhat different realizations of the observations $\mathbf{y}_i$:

$$\mathbf{x}_i^a = \mathbf{x}_i^b + \hat{\mathbf{K}}\left(\mathbf{y}_i - H\left(\mathbf{x}_i^b\right)\right), \quad (4)$$

where H is the observation operator that maps the model states to the observation space. In (4), $\mathbf{y}_i = \mathbf{y} + \mathbf{y}_i'$ are perturbed observations from observation $\mathbf{y}$, which is assumed to have normal distribution with mean equal to $\mathbf{y}$ and covariance equal to $\mathbf{R}$. From the ensemble of observation perturbations, the estimated observational error covariance $\hat{R}$ is constructed as

$$\hat{R} = \frac{1}{N-1}\mathbf{y}'\mathbf{y}'^{\mathrm{T}} \quad (5)$$

The gain matrix $\hat{K}$ in (4) is defined as

$$\hat{\mathbf{K}} = \hat{\mathbf{P}}^b H^T\left(H\hat{\mathbf{P}}^b H^T + \mathbf{R}\right)^{-1}, \quad (6)$$

which is similar to that in the Kalman filter but permitting a possibly nonlinear H and using the ensemble to estimate the forecast error covariance $\hat{\mathrm{P}}^{\mathrm{b}}$ and the observational error covariance $\hat{\mathrm{R}}$. The gain matrix can be formed without ever explicitly estimating and storing the full forecast error covariance $\hat{\mathrm{P}}^{\mathrm{b}}$ but using the following equations to calculate $\hat{\mathrm{P}}^{\mathrm{b}}H^{\mathrm{T}}$ and $H\hat{\mathrm{P}}^{\mathrm{b}}H^{\mathrm{T}}$ directly [*Evensen*, 1994; *Houtekamer and Mitchell*, 1998]:

$$\hat{\mathbf{P}}^{\mathrm{b}}H^T = \frac{1}{N-1}\sum_{i=1}^{N}\mathbf{x}_i'^{\mathrm{b}}\left(H\left(\mathbf{x}_i'^{\mathrm{b}}\right) - \overline{H(\mathbf{x}^{\mathrm{b}})}\right)^{\mathrm{T}}, \quad (7)$$

$$H\hat{\mathbf{P}}^{\mathrm{b}}H^{\mathrm{T}} = \frac{1}{N-1}\sum_{i=1}^{N}\left(H\left(\mathbf{x}_i^{\mathrm{b}}\right) - \overline{H(\mathbf{x}^{\mathrm{b}})}\right)\left(H\left(\mathbf{x}_i'^{\mathrm{b}}\right) - \overline{H(\mathbf{x}^{\mathrm{b}})}\right)^{\mathrm{T}}. \quad (8)$$

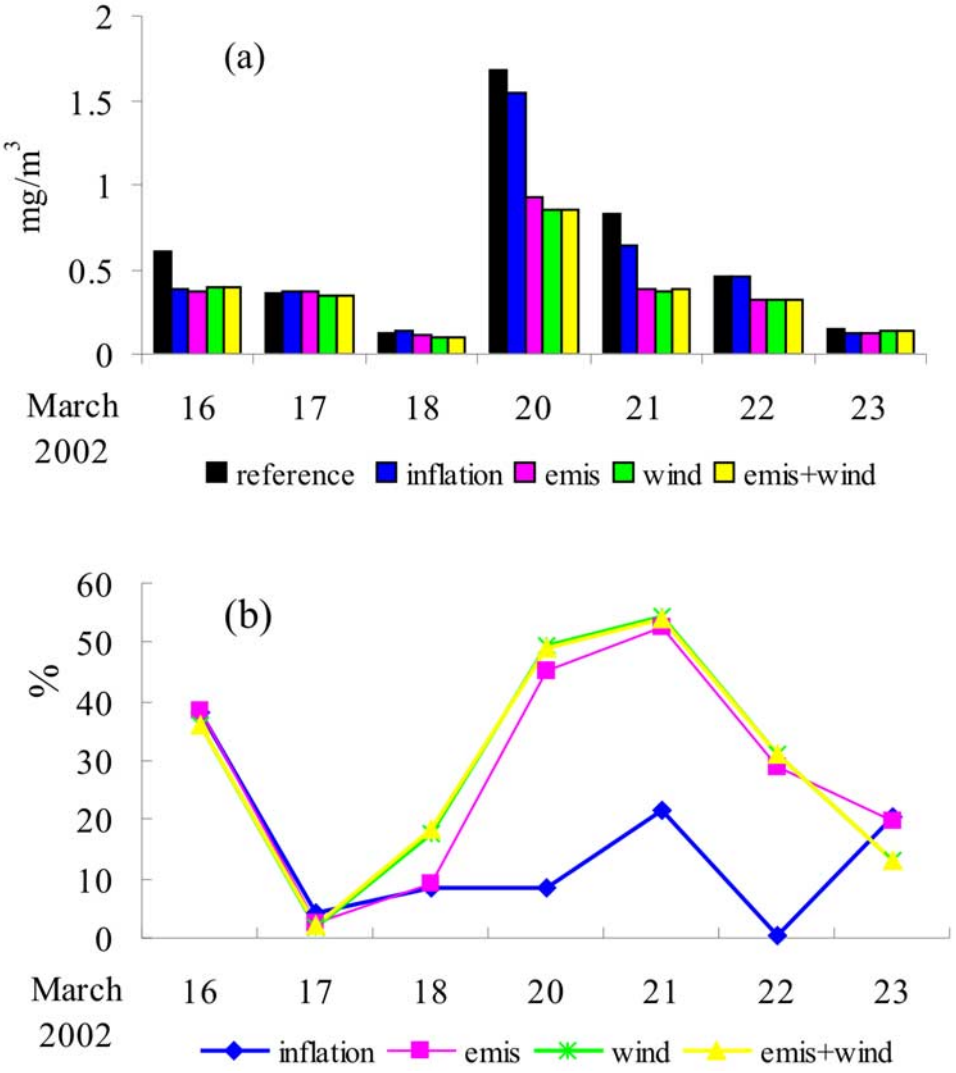

Figure 6. (a) RMS errors between observed daily mean PM_{10} and 24-h averaged forecast of dust aerosol concentrations (d < 10 μm) for each experiment. (b) Percentages of reduced RMS errors relative to that of the control run.

In (7) and (8),

$$\overline{H(\mathbf{x}^{\mathrm{b}})} = \frac{1}{N}\sum_{i=1}^{N} H\left(\mathbf{x}_i^{\mathrm{b}}\right).$$

Once each member is updated, we take the mean $\bar{\mathbf{x}}^a = \frac{1}{N}\sum_{i=1}^{N}\mathbf{x}_i^a$ as the analysis.

[13] The method described above is the traditional EnKF described by *Evensen* [1994], in which the background error covariance estimated directly from an ensemble of forecasts propagated forward from an ensemble of analyses using the fully nonlinear forecast model misses the extra model error covariance. Hence the analysis errors may be underestimated, and then the forecast errors may be underestimated in the following cycle, so that less weight is given to the new observations. This process can feed back on itself, with the ensemble assimilation method progressively ignoring observational data more and more in successive cycles, leading eventually to a useless ensemble, i.e., filter divergence [e.g., *Houtekamer and Mitchell*, 1998]. The phenomenon is also found in previous dust-storm data assimilation using EnKF [*Lin et al.*, 2008a].

[14] Scientists have been trying to incorporate noise into the ensemble of forecasts so that they account for model error. One simple method used to remedy this problem is the covariance inflation to increase the error [*Anderson*, 2001; *Hamill et al.*, 2001]. In previous dust-storm data assimilation [*Lin et al.*, 2008a], filter divergence is also avoided by introducing an inflation factor f ($f \geq 1$) to increase the ensemble variance appropriate to the missing model error covariance, so that formula (6) is rewritten as

$$\hat{\mathbf{K}} = f\hat{\mathbf{P}}^b H^T\left(fH\hat{\mathbf{P}}^b H^T + \hat{\mathbf{R}}\right)^{-1}. \quad (9)$$

The inflation factor is selected empirically in order to maintain sufficient covariance and draw more to the observations. However, this does not change the subspace spanned by the ensemble and does not account for the

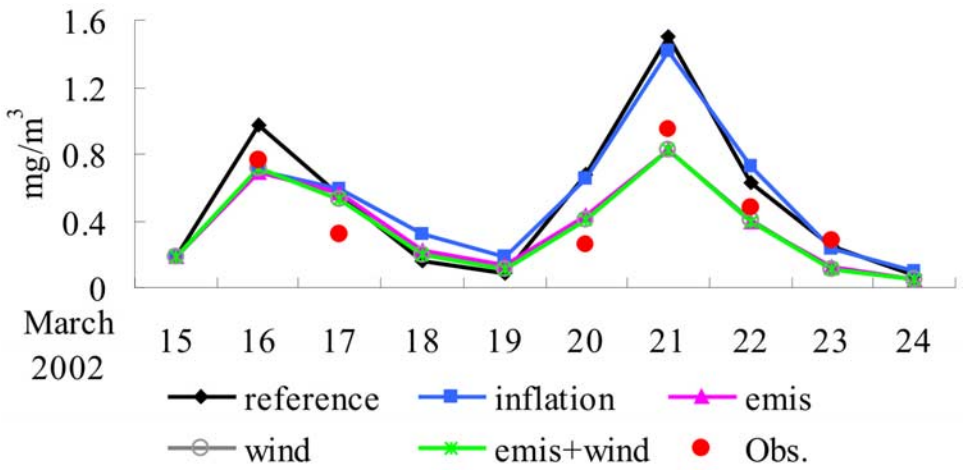

Figure 7. Comparison of observed daily mean PM_{10} (red dots) and 24-h averaged forecast of surface dust aerosol concentrations (d < 10 μm) in Beijing for "reference" (black), "inflation" (blue), "emis" (pink), "wind" (gray), and "emis + wind" (green).

model error from the origin. If the model error projects into a substantially different subspace, this method may not be effective. More sophisticated approaches to this problem are appropriate, especially when dealing with models that have significant systematic errors. Dust storm is a fast transient process, in which the expected and reasonable forecast error variance should increase with the dust onset and decrease with its cessation automatically. Hence looking for the origin of model error and accounting for them accurately is more appropriate for assimilation and for forecast improvement.

[15] In fact, the EnKF more easily accounts for the model uncertainty than other assimilation techniques. The EnKF not only can be used for initial state estimation but also can readily include parameter estimation by state-space augmentation in the same frame work [*Annan et al.*, 2005; *Evensen*, 2006]. The principle is to consider the parameters as part of the model state alongside the conventional variables, and then using the covariance estimated from the ensemble to update parameters directly in the same manner as for the state variables. So we can use EnKF to account for the model uncertainty and modify the model bias in the same manner as for parameter estimation.

3.2. Experimental Details

[16] As mentioned in the introduction, this paper will focus on model bias correction in heavy dust episodes by introducing model uncertainty into the EnKF assimilation, and examine whether it can also avoid filter divergence reasonably without variance inflation.

[17] Preliminary sensitivity analysis of model uncertainty [*Lin et al.*, 2008b], including their biases, for the dust transport model [*Wang et al.*, 2000] over north China, suggests that dust emissions, surface wind fields and dry deposition velocity all have a strong impact on surface dust prediction and have large biases. Among these, the impact of dry deposition velocity is much smaller than any other one and its turbulent part is also influenced by the friction velocity which is calculated by the surface winds. Therefore only the uncertainties of dust emission Q and surface wind fields $\vec{V}$ are considered for bias correction.

[18] Two ensemble parameters $\boldsymbol{\alpha}_{\mathrm{Q}} = (\alpha_{\mathrm{Q1}}, \alpha_{\mathrm{Q2}}, \cdots, \alpha_{\mathrm{Q}N})$ and $\boldsymbol{\alpha}_{\mathrm{V}} = (\alpha_{\mathrm{V1}}, \alpha_{\mathrm{V2}}, \cdots, \alpha_{\mathrm{V}N})$ are selected to represent these two uncertainties (N is the ensemble size equal to 50), which are nondimensional linear multipliers of dust emission intensity $Q_{i,j,l}$ and surface wind fields $\vec{V}_{i,j}$ respectively at each grid point over the numerical domain:

$$Q^{new}_{i,j,l,k} = \alpha_{\mathrm{Q}k} * Q_{i,j,l}, \tag{10}$$

$$\vec{\mathbf{V}}^{new}_{i,j,k} = \alpha_{\mathbf{V}k} * \vec{\mathbf{V}}_{i,j}, \tag{11}$$

where i, j is the location, l is the l-th size bin and k is the ensemble member ($k = 1, \ldots, N$). The initial ensembles of parameter $\boldsymbol{\alpha}_{\mathrm{Q}}$ and $\boldsymbol{\alpha}_{\mathrm{V}}$ are assumed to be drawn from the normal distribution with mean equal to the original value 1 and standard deviation equal to 20%. The standard deviation (20%) is a conservative estimate.

[19] Three EnKF schemes (given as "emis", "wind", and "emis + wind" and shown in Table 2) are designed to assimilate these two parameters individually and simultaneously to compare their impacts on heavy dust forecast and correct their biases. These three EnKF schemes not only provide initial conditions but also correct the model bias by accounting for the uncertainty into the assimilation cycles. The scheme "emis" and "wind" consider the uncertainty of dust emissions and surface wind speed respectively. The scheme "emis + wind" considers these two uncertainties simultaneously. Because the friction velocity is calculated by the surface wind fields, its bias is also modified when the surface wind fields are corrected. Parameters are updated in the same manner as the model states by augmenting them to the control variables $\hat{\mathbf{X}}^{\mathrm{b}}$ in EnKF as shown in formula (12):

$$\hat{\mathbf{X}}^{\mathrm{b}} = \begin{pmatrix} \mathbf{x}_1, \ldots, \mathbf{x}_N \\ \alpha_{\mathrm{Q1}}, \cdots, \alpha_{\mathrm{Q}N} \\ \alpha_{\mathrm{V1}}, \cdots, \alpha_{\mathrm{V}N} \end{pmatrix} \tag{12}$$

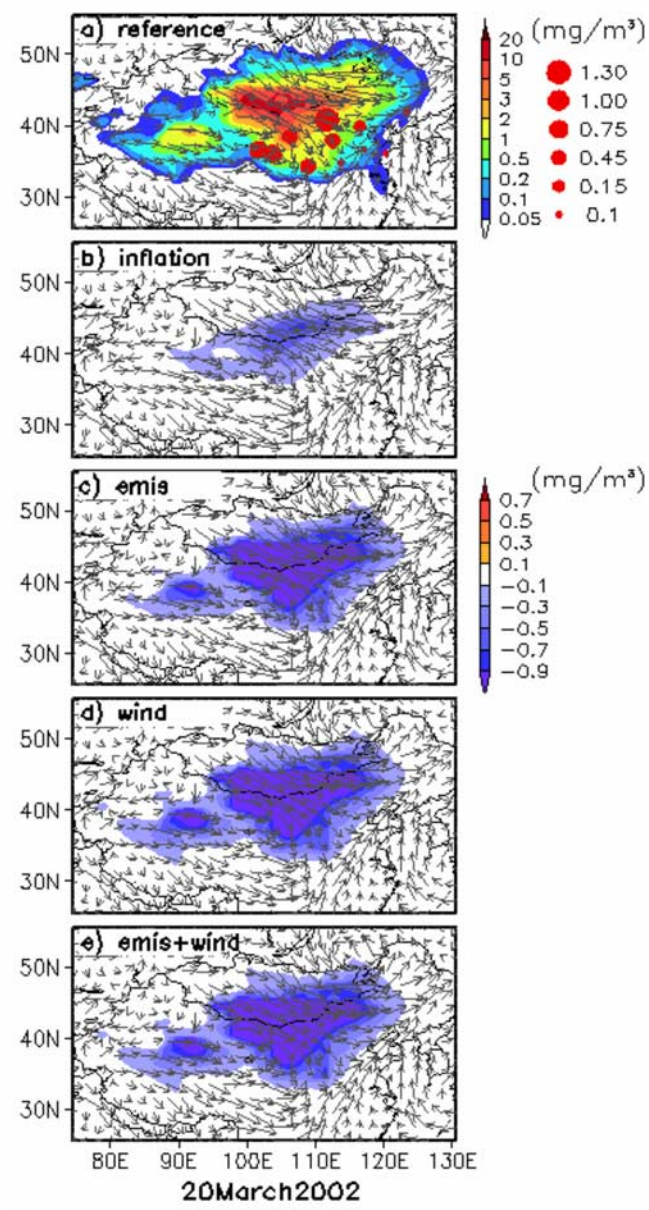

Figure 8. Surface distribution of 24-h averaged forecasts of dust aerosol concentrations (d < 10 μm) without assimilation (a), and the difference between situations with and without assimilation ((b), (c), (d), and (e) for the schemes "inflation", "emis", "wind", and "emis + wind", respectively) on 20 March. The closed red circles represent the observed PM_{10} levels. Surface wind fields in Figures 8d and 8e are the corrected winds.

If not assimilated, the parameters are held to be at the default value of one.

[20] In order to demonstrate and compare the impact of the model uncertainty and their biases on assimilation and on the forecasts, we include two other schemes: one is the reference run without assimilation ("reference") and the other is the EnKF scheme with variance inflation but without model uncertainty ("inflation"). More details of the inflation scheme are discussed by *Lin et al.* [2008a].

[21] In this study, the initial background ensemble perturbations of the model state are generated by adding random amplitude and phase shifts to the first-guess $\mathbf{x}(x, y, z)$ as follows:

$$\mathbf{x}_i(x,y,z) = (1+\delta_i)\mathbf{x}(x+\varepsilon_i, y+\omega_i, z+\eta_i) \qquad (13)$$

where,

$$\delta \in N\left(0,a^2\right), \varepsilon \in N\left(0,l_x^2\right), \omega \in N\left(0,l_y^2\right), \eta \in N\left(0,l_z^2\right),$$

and $i = 1, \cdots, N(N = 50)$. The observations are also perturbed from the normal distribution $N(0, \mathbf{R})$. The observational error covariance R is assumed to be a diagonal matrix with its standard deviation set at 10% of the observation.

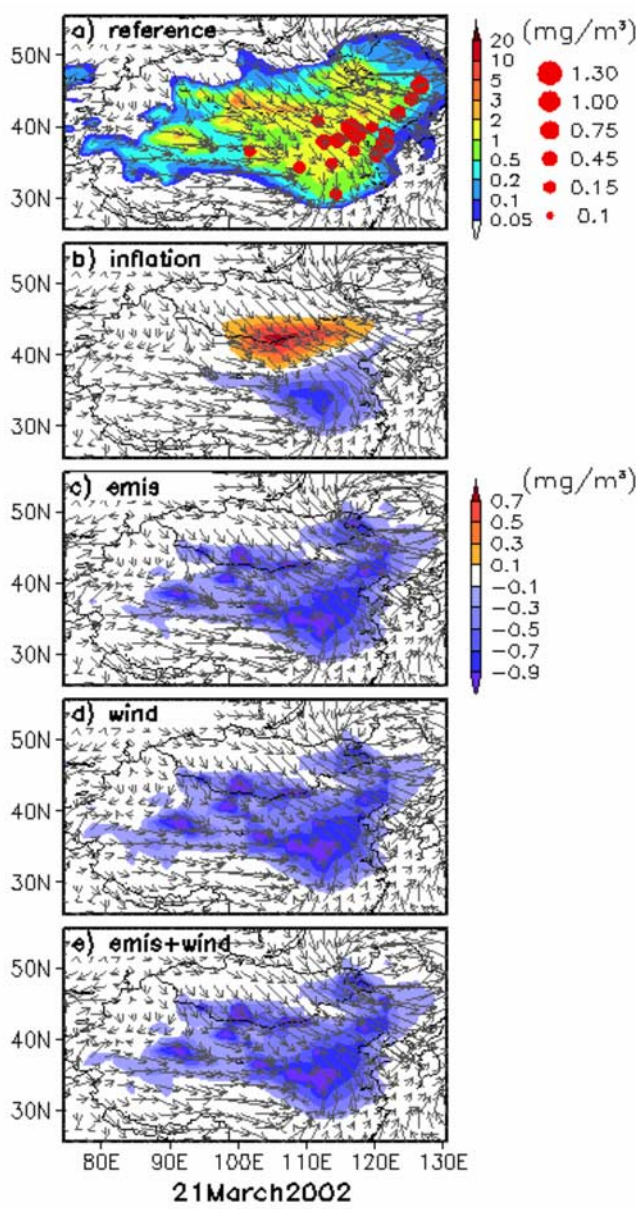

Figure 9. As in Figure 8 but on 21 March 2002.

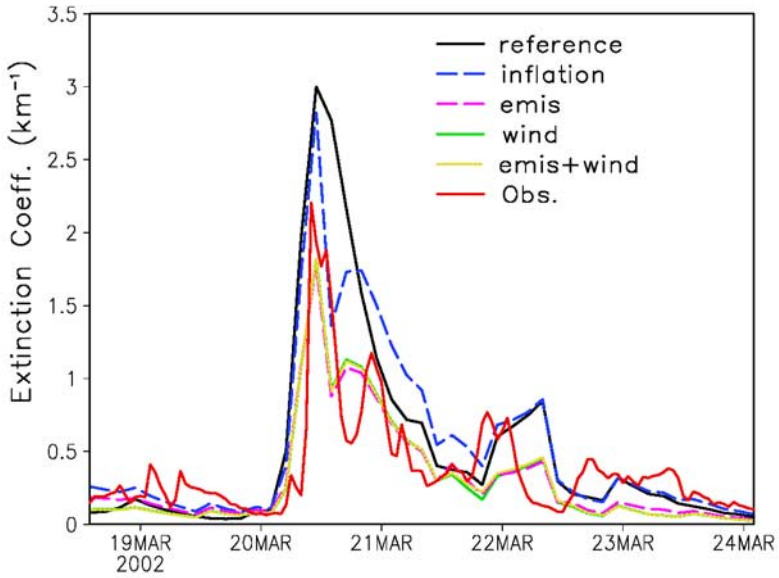

Figure 10. Dust extinction coefficients observed by NIES lidar and predicted by the model in different experiments in Beijing.

[22] Since the values for model state (dust concentrations) and parameters should be positive, negative analyses will be replaced with zero.

4. Results and Discussions

[23] As stated in previous sections, we specially use EnKF to correct model biases and examine their impacts on heavy dust-storm forecasting. The assimilation cycles are performed once a day during 15–24 March 2002, which have two dust onsets observed over a wide area including China, Korea and Japan [*Shao et al.*, 2003; *Sugimoto et al.*, 2003].

[24] First examined is the spread estimated directly from the finite ensemble forecasts, which represent the forecast uncertainty in EnKF. If the spread is underestimated, filter divergence will occur with the analysis far away from the observations. The root mean square (RMS) spreads of the ensemble forecasts of surface dust concentrations are shown in Figure 2. The blue line shows the RMS spread in scheme "inflation", which includes the value before and after inflation linked by the dotted line after two cycles. Obviously, if not inflated, it decreases quickly with assimilation cycles and leads to filter divergence. Taking the uncertainty of dust emissions and surface wind fields into account, the spread can increase automatically when a new episode starts on 19 March 2002 without inflation (pink, green, and yellow ones). Moreover, except for the magnitude, the horizontal distribution and the maximum center of the spread in these three experiments is much more reasonable than that in scheme "inflation" compared with the distribution of dust concentrations (Figures 3 and 4). When taking the model uncertainty into account, the maximum center of forecast error (spread) estimated from the ensemble located near the source region and the maximum dust concentration in schemes.

[25] Figure 5 indicates the horizontal distribution of estimated dust emission intensity for the reference run without assimilation (a) and the difference between situations without and with assimilation along with model bias correction (b, c and d) during the period of 15–24 March 2002 (10 d). Since the scheme "inflation" does not correct the dust emission intensity, the results are the same as for the reference run, and therefore are not shown here. The total dust emissions during the period are about 164.3 Tg for the reference run. The emissions are decreased to about 110.4 Tg (33% decrease), 101.8 Tg (38% decrease) and 102.6 (38% decrease) Tg for the assimilation schemes "emis", "wind", and "emis + wind" respectively after correcting the bias.

[26] Figure 6a shows the RMS error between observed daily mean PM_{10} levels and 24-h averaged forecasts of dust concentrations ($d < 10\ \mu m$) (RMS error of innovations). The forecasts of dust concentrations of EnKF assimilation schemes used for comparison hereinafter are the ensemble mean of the forecasts after assimilation. When dust-storms are heavy the RMS error of the "inflation" scheme is slightly reduced compared with that of the control run ("reference"), while the RMS errors of scheme "emis", "wind", and "emis + wind" are much more reduced than that in the scheme "inflation" especially after several cycles. The RMS errors relative to the control run are reduced by more than 45% (0.75 $mg \cdot m^{-3}$) on 20 March and 50% (0.41 $mg \cdot m^{-3}$) on 21 March in the "emis", "wind", and "emis + wind" scheme, while they are only reduced by about 8% and 20% in the "inflation" scheme (Figure 6b). This indeed indicates that, by considering the model uncertainty in the assimilation schemes, the spread is more reasonable and accurate to represent the forecast error than that by inflation. this then leads to more significant improvement of forecasts.

[27] Figure 7 shows the observed daily mean PM_{10} and the 24-h averaged forecast of surface concentrations of each experiment in Beijing. The observations are only shown on days when they pass through the quality control. The daily

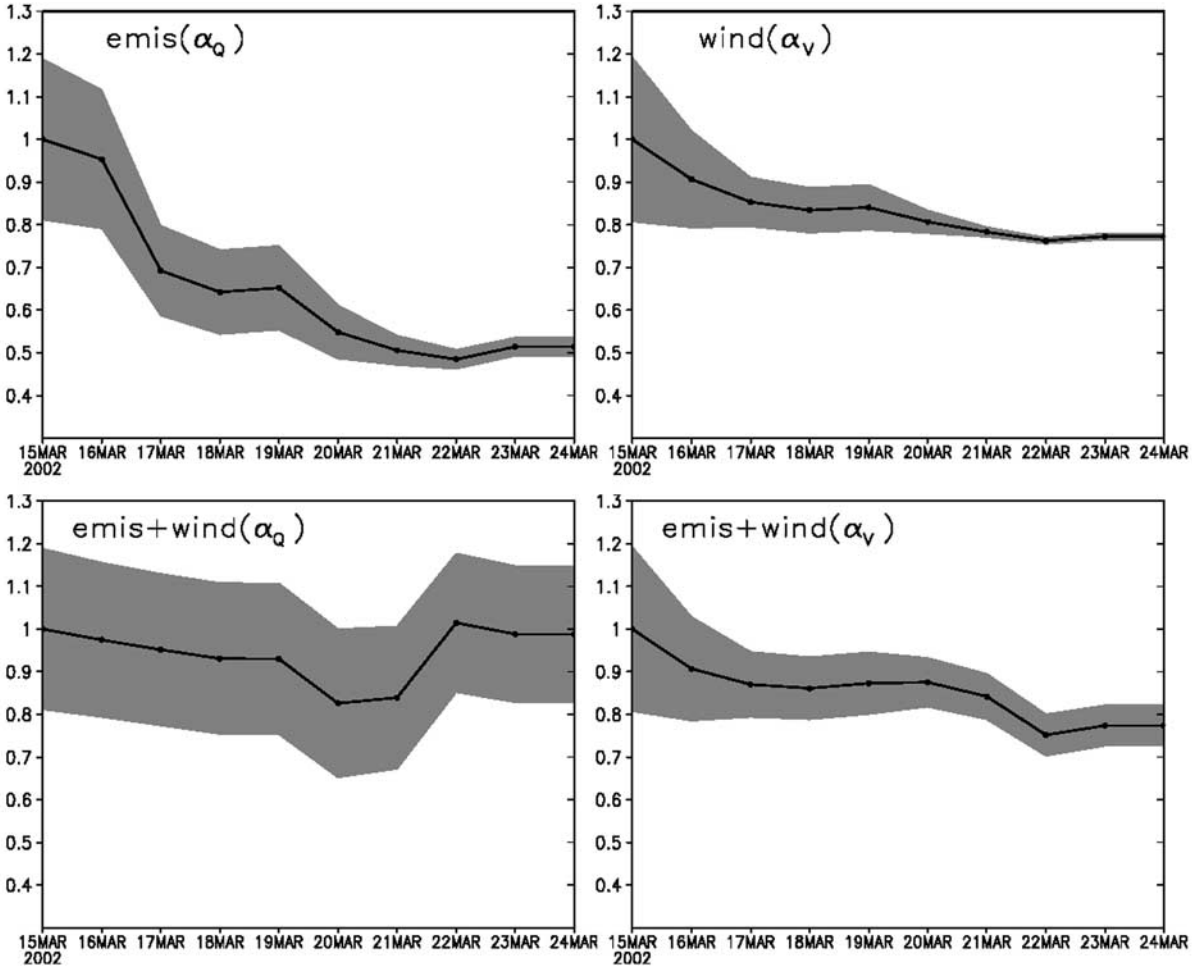

Figure 11. Convergence of the parameter α_Q (left) in the schemes "emis" and "emis + wind", and α_V (right) in the schemes "wind" and "emis + wind". Solid lines show the ensemble means and shaded areas represent their ensemble spreads (standard deviation).

averaged prediction after assimilation of scheme "inflation" (blue one) becomes similar with that of the reference run (black one), while the prediction of scheme "emis" (pink one), "wind" (gray one), and "emis + wind" (green one) are still much closer to the observation than that of the control run and scheme "inflation" especially after several cycles. The reasons for the similarities of the "emis", "wind", and "emis + wind" schemes will be discussed together with the bias correction.

[28] In addition, the 24-h averaged forecasts of surface dust concentrations are much improved after considering the model uncertainty. Surface distributions of 24-h averaged forecasts of dust aerosol concentrations ($d < 10\ \mu m$) without assimilation and the difference between situations with and without assimilation for each experiment on 20 and 21 March are shown in Figures 8 and 9 respectively. Compared with the PM_{10} observations, the forecast concentrations without assimilation (Figures 8 and 9a) are much larger than the observations, especially in the north part of North China. On 20 March, only the PM_{10} observation in Hohhot (1.35 $mg \cdot m^{-3}$) exceeds 1 $mg \cdot m^{-3}$, while the middle and west part of Inner Mongolia, Gansu, Shaanxi, Ningxia and Shanxi provinces etc. are covered by modeled dust with concentrations of more than 2 $mg \cdot m^{-3}$. On 21 March, most of the forecast concentrations of the control run are larger than 1 $mg \cdot m^{-3}$ over North China, while only the PM_{10} observation in Tianjin exceeds 1 $mg \cdot m^{-3}$. After EnKF assimilation the 24-h averaged forecasts of surface concentrations decrease (Figures 8 and 9b, 9c, 9d, and 9e for scheme "inflation", "emis", "wind" and "emis + wind" respectively). It can also be seen that the concentrations are much decreased and significantly improved after taking the model uncertainty into account ((c), (d) and (e)). In (d) and (e), the surface wind fields are the corrected winds with the speed reduced by about 20% and 13% on 20 March, and 22% and 16% on 21 March for the schemes "wind" and "emis + wind", respectively.

[29] To further check the results from these experiments, we use an independent NIES lidar observation in Beijing for verification. Figure 10 shows the time variation of surface dust extinction coefficients observed by NIES lidar and predicted by the model in Beijing. Observed dust extinction coefficients show a very sharp increase on the morning of 20 March as simulated by the model. In addition, the lidar

observations have two peaks on 20 March, one large in the morning and one small in the night, which agrees well with the variation of Total Suspended Particle (TSP) observed on that day by Beijing Normal University [*Zhao et al.*, 2007]. Nevertheless, the prediction without assimilation just shows one single peak on 20 March. After EnKF assimilation, the two obvious peaks of the forecasts appear on 20 March in the four assimilation schemes. One possibility of the second peak after assimilation is partly caused by a plume that has traveled longer than the plume causing the large peak. For the coefficient levels, they are much improved only after considering the model uncertainty in the last three experiments.

[30] A significant improvement in modeling abilities by considering model uncertainty in the EnKF assimilation is described above. Next we will investigate the convergence of the two parameters and the correction of their biases. Figure 11 shows the convergence of parameters α_Q (left) and α_V (right) and their spreads estimated during the EnKF assimilation cycles. Parameters α_Q converge to about 0.5 in scheme ''emis'' and α_V converge to 0.76 in scheme ''wind'', agreeing well with the results in preliminary analyses of uncertainty for this model (0.4 and 0.7 for parameter α_Q and α_V respectively). This result indicates that we can accurately modify the model bias by assimilating the parameters. The shade areas become narrower with assimilation cycles, which imply that the uncertainty of dust emissions and wind fields have decreased. In the scheme ''emis + wind'', when accounting for the two kinds of model uncertainty simultaneously, parameters α_Q and α_V do not converge to the same result when each is corrected individually. The overall impact of the uncertainty of dust emissions and surface wind speeds indicates that they can compensate for each other. The uncertainty of surface wind speed is decreased but not the uncertainty of dust emission in scheme ''emis + wind'', which indicates that the impact of uncertain wind is larger than that of uncertain dust emission.

[31] The results of the schemes accounting for model uncertainty and correcting for their biases seem quite similar because they influence the dust concentrations in very similar ways. Scheme ''emis'' directly adjusts the dust emission amount by assimilating concentration observations. Scheme ''wind'' adjusts the surface wind field and results in the adjustment of the dust emission amount. This is because the dust emission amount is calculated in the model by a parameterization scheme that largely depends on friction velocity, which is also adjusted by surface wind fields. The surface wind fields play little role in the transport of the large scale dust storms that are mainly transported by higher level wind fields. Therefore scheme ''emis'' and ''wind'' have similar impacts on dust concentrations. Scheme ''emis + wind'', a combination of scheme ''emis'' and ''wind'', performs similarly to scheme ''emis'' and ''wind''.

[32] In this study, the bias of the surface wind speed is corrected by the assimilation. In addition, the surface friction velocity is also corrected based on the wind field correction. The dust emissions and the horizontal transport are dominantly controlled by the wind fields. Despite the modeling or the observations, the errors of winds exist as a result of several factors such as model uncertainties and representative error of observations. The wind fields from the MM5 mesoscale model are inputs of our dust transport model and the uncertainties in the wind fields still exist to some extent. On the basis of our past sensitivity analyses of the model uncertainty of the dust transport model, we found that the uncertainty of the surface wind speed has a strong impact on the forecasts, and it is also large for the case in this study. The reasons for the errors in wind fields could be the lack of sufficient vertical resolution in MM5, errors in the boundary layer parameterizations, and lack of meteorological observations. Here the reason why we discuss the correction of wind fields is to find a way through the revision of dynamic wind fields to correct the dust emission amount and to explore the impact of wind field correction in the context of dust storm simulations. The satisfaction of mass continuity by this the approach was fit by the revision of vertical velocity through the mass continuity formula.

5. Conclusions

[33] In this study we focused on dust model bias correction with implementation of several data assimilation schemes based on the EnKF method. The data assimilation experiments are performed in a 10-d period in March 2002 when there were two severe dust storm episodes over north China.

[34] Through the numerical simulation, it is found that the forecasts are not significantly improved, although the EnKF with inflation and without model errors can avoid filter divergence and improve the initial conditions of dust concentration. When the model error and their biases in the dust emission and the surface wind are considered in the data assimilation scheme, the forecast spreads can be maintained at a reasonable level compared with the RMS error of innovations. Moreover, the ensemble spread can increase automatically when another new dust episode starts. The data assimilation schemes with bias correction can significantly improve the 24-h forecasts. The RMS error of 24-h averaged forecast is reduced by more than 45% (0.75 $mg.m^{-3}$) on 20 March and 50% (0.41 $mg.m^{-3}$) on 21 March after correcting the biases. The total dust emissions are reduced by more than 33% (53.9 Tg). These indicate that the biases in dust emissions and surface wind are two important sources of forecast errors. When bias correction of dust emissions and the surface wind fields are performed simultaneously, they do not converge to the same values as when each bias correction is performed individually. This, together with their similar impacts on surface concentration fields, indicates that they can compensate each other.

[35] Although the large biases in dust emissions and wind fields are common in other dust transport models as reviewed in the introduction, model bias correction is highly model-dependent and this study is only for one model. However, based on careful analysis of model errors and their biases for a given model, this method can be easily extended to other models. Certainly, there could be some other important model biases in addition to dust emission and wind field. Correcting them accurately will improve dust storm forecasts. This study is only a first step toward this goal using EnKF.

[36] **Acknowledgments.** The authors wish to thank anonymous reviewers for their comments and suggestions. This study was supported by the Chinese Academy of Sciences (KZCX2-YW-202, KZCX2-YW-205) and the Natural Science Foundation of China (40437017/40221503/40533017) and the MOST (20060106A3004 and 2005CB422205).

References

Anderson, J. L. (2001), An ensemble adjustment Kalman filter for data assimilation, *Mon. Weather Rev.*, *129*, 2884–2903.

Annan, J. D., J. D. Lunt, J. C. Hargreaces, and P. J. Valdes (2005), Parameter estimation in an atmospheric GCM using the Ensemble Kalman Filter, *Nonlin. Process. Geophys.*, *12*, 363–371.

Evensen, G. (1994), Sequential data assimilation with a nonlinear quasi-geostrophic model using Monte Carlo methods to forecast error statistics, *J. Geophys. Res.*, *99*(C5), 10,143–10,162.

Evensen, G. (2006), *Data Assimilation: The Ensemble Kalman Tilter*, Springer, Germany.

Gong, S. L., X. Y. Zhang, T. L. Zhao, I. G. McKendry, D. A. Jaffe, and N. M. Lu (2003), Characterization of soil dust aerosol in China and its transport and distribution during 2001 ACE-Asia: 2. Model simulation and validation, *J. Geophys. Res.*, *108*(D9), 4262, doi:10.1029/2002JD002633.

Hamill, T. M., J. S. Whitaker, and C. Snyder (2001), Distance-dependent filtering of background error covariance estimates in an ensemble Kalman filter, *Mon. Weather Rev.*, *129*, 2776–2790.

Hanna, S. R., Z. Lu, H. C. Frey, N. Wheeler, J. Vukovich, S. Arunachalam, M. Fernau, and D. A. Hansen (2001), Uncertainties in predicted ozone concentrations due to input uncertainties for the UAM-V photochemical grid model applied to the July 1995 OTAG domain, *Atmos. Environ.*, *35*, 891–903.

Houtekamer, P. L., and H. L. Mitchell (1998), Data assimilation using an ensemble Kalman filter technique, *Mon. Weather Rev.*, *126*, 796–811.

Huebert, B. J., T. Bates, P. B. Russell, G. Shi, Y. J. Kim, K. Kawamura, G. Carmichael, and T. Nakajima (2003), An overview of ACE-Asia: Strategies for quantifying the relationships between Asian aerosols and their climatic impacts, *J. Geophys. Res.*, *108*(D23), 8633, doi:10.1029/2003JD003550.

Lin, C., Z. Wang, and J. Zhu (2008a), An Ensemble Kalman Filter for severe dust storm data assimilation over China, *Atmos. Chem. Phys.*, *8*, 2975–2983.

Lin, C. Y., J. Zhu, and Z. F. Wang (2008b), Uncertainty analysis of a dust transport model, *Chinese J. Atmos. Sci.* (in Chinese), in press.

Mallet, V., and B. Sportisse (2006), Uncertainty in a chemistry-transport model due to physical parameterizations and numerical approximations: An ensemble approach applied to ozone modeling, *J. Geophys. Res.*, *111*, D01302, doi:10.1029/2005JD006149.

Schmidt, H. (2002), Sensitivity studies with the adjoint of a chemistry transport model for the boundary layer, in *Air Pollution Modelling and Simulation*, edited by B. Sportisse, pp. 400–410, Springer, New York.

Shao, Y., et al. (2003), Northeast Asian dust storms: Real-time numerical prediction and validation, *J. Geophys. Res.*, *108*(D22), 4691, doi:10.1029/2003JD003667.

Sugimoto, N., I. Uno, M. Nishikawa, A. Shimizu, I. Matsui, X. Dong, Y. Chen, and H. Quan (2003), Record heavy Asian dust in Beijing in 2002: Observations and model analysis of recent events, *Geophys. Res. Lett.*, *30*(12), 1640, doi:10.1029/2002GL016349.

Uematsu, M., Z. Wang, and I. Uno (2003), Atmospheric input of mineral dust to the western North Pacific region based on direct measurements and a regional chemical transport model, *Geophys. Res. Lett.*, *30*(6), 1342, doi:10.1029/2002GL016645.

Uno, I., et al. (2006), Dust model intercomparison (DMIP) study over Asia: Overview, *J. Geophys. Res.*, *111*, D12213, doi:10.1029/2005JD006575.

Wang, Z. F., H. Ueda, and M. Y. Huang (2000), A deflation module for use in modeling long-range transport of yellow sand over East Asia, *J. Geophys. Res.*, *105*, 26,947–26,958.

Wang, Z., H. Akimoto, and I. Uno (2002), Neutralization of soil aerosol and its impact on the distribution of acid rain over East Asia: Observations and model results, *J. Geophys. Res.*, *107*(D19), 4389, doi:10.1029/2001JD001040.

Zhao, X. J., G. S. Zhuang, Z. F. Wang, Y. L. Sun, Y. Wang, and H. Yuan (2007), Variation of sources and mixing mechanism of mineral dust with pollution aerosol-revealed by the two peaks of a super dust storm in Beijing, *Atmos. Res.*, *84*, 265–279.

C. Lin, Z. Wang, and J. Zhu, State Key Laboratory of Atmospheric Boundary Layer Physics and Atmospheric Chemistry (LAPC), Institute of Atmospheric Physics, Chinese Academy of Sciences, P.O. Box 9804, Huayan Li No. 40, Qijiahuozi, Deshengmen Wai Avenue, Beijing 100029, China. (cylin@mail.iap.ac.cn; zifawang@mail.iap.ac.cn; jzhu@mail.iap.ac.cn)